Surface Science 651 (2016) 76–83

Contents lists available at ScienceDirect

Surface Science

journal homepage: www.elsevier.com/locate/susc

Adjusting island density and morphology of the $SrTiO_3(110)$-(4×1) surface: Pulsed laser deposition combined with scanning tunneling microscopy

Stefan Gerhold [a], Michele Riva [a,*], Bilge Yildiz [a,b], Michael Schmid [a], Ulrike Diebold [a]

[a] Institute of Applied Physics, TU Wien, Wiedner Hauptstrasse 8-10/E134, A-1040 Vienna, Austria
[b] Laboratory for Electrochemical Interfaces, Department of Nuclear Science and Engineering, Massachusetts Institute of Technology, 77 Massachusetts Avenue, Cambridge, MA 02139, United States

ARTICLE INFO

Article history:
Received 15 February 2016
Accepted 10 March 2016
Available online 16 March 2016

Keywords:
STM
Oxides
Growth
RHEED
PLD

ABSTRACT

The first stages of homoepitaxial growth of the (4×1) reconstructed surface of $SrTiO_3(110)$ are probed by a combination of pulsed laser deposition (PLD) with *in-situ* reflection high energy electron diffraction (RHEED) and scanning tunneling microscopy (STM). Considerations of interfacing high-pressure PLD growth with ultra-high-vacuum surface characterization methods are discussed, and the experimental setup and procedures are described in detail. The relation between RHEED intensity oscillations and ideal layer-by-layer growth is confirmed by analysis of STM images acquired after deposition of sub-monolayer amounts of $SrTiO_3$. For a quantitative agreement between RHEED and STM results one has to take into account two interfaces: the steps at the circumference of islands, as well as the borders between two different reconstruction phases on the islands themselves. Analysis of STM images acquired after one single laser shot reveals an exponential decrease of the island density with increasing substrate temperature. This behavior is also directly visible from the temperature dependence of the relaxation times of the RHEED intensity. Moreover, the aspect ratio of islands changes considerably with temperature. The growth mode depends on the laser pulse repetition rate, and can be tuned from predominantly layer-by-layer to the step-flow growth regime.

1. Introduction

Pulsed laser deposition (PLD) has emerged as the predominant tool for the growth of high-quality films of complex oxides. In particular the growth of layered heterostructures is relatively simple, since it only requires switching between the target materials [1,2]. Another advantage of PLD is its highly out-of-equilibrium growth condition. The high instantaneous flux leads to nucleation of a high number of islands, favoring kinetically-limited 2D growth [3]. This is especially relevant for those heterostructures in which the growing material tends to follow a 3D growth in close-to-equilibrium conditions.

Oxide PLD is rarely combined with surface analysis techniques, although they provide invaluable atomic-scale information concerning the prominent influence of surface and interface effects on both, the growth phenomena and the resulting material properties. Conversely, surface science needs 'model' samples, where structure, stoichiometry, and defects are well controlled; this can, in principle, be provided by PLD heteroepitaxy for almost any kind of material. As complex multicomponent oxides are at the heart of emerging applications in energy- and information-related research [4,5], surface investigations of epitaxial films should be particularly promising in unraveling the molecular-scale surface processes that are central to device functionality. In the literature, only few studies report on results obtained by combining PLD growth with *in-situ* scanning tunneling microscopy (*i.e.*, conveniently in the same UHV setup, without breaking vacuum). Both homoepitaxial growth of $SrTiO_3$ (short STO) (001) [6,7] and heteroepitaxial growth of other perovskites [8–10] were reported. One technical challenge lies in the fact that surface science, and in particular highly resolved STM, require the PLD process to fulfill stringent conditions of chemical purity. The present paper reports some technical improvements aimed at achieving such conditions, and shows the prowess of combining reflection high-energy electron diffraction (RHEED)-controlled PLD and STM analysis for achieving exquisite control over oxide surface structure and morphology.

* Corresponding author.
E-mail address: riva@iap.tuwien.ac.at (M. Riva).

http://dx.doi.org/10.1016/j.susc.2016.03.010

The perovskite $SrTiO_3$ has evolved as a prototype for complex oxides, *i.e.*, oxidic compounds hosting more than one cationic species [6,7,11–14]. This study follows the homoepitaxial growth of $SrTiO_3$ on the (110) surface. Homoepitaxy provides the advantage of performing growth studies unaffected by misfit strain between substrate and film. Although PLD is often reported to readily produce high-quality thin films, it was shown that only a precise tuning of the growth parameters leads to deposited films with properties comparable to those of the underlying substrate, even in the case of homoepitaxy [15–17]. These parameters include the background gas pressure and composition, substrate temperature, target-to-substrate distance and alignment, UV laser fluence, pulse duration and repetition rate, and ablation area. The present paper investigates the effects of the substrate temperature and the UV laser repetition rate on the growth.

Our group has studied the surface structure and chemistry of $SrTiO_3$(110) in detail in previous works and we have shown that the (4×1) surface has the advantages of high stability, inertness, and well-reproducible preparation [18–23]. Here the focus is on the results from the early stages of film growth, and on producing well-characterized (4×1) surfaces by PLD. Freshly preparing and characterizing the substrate STO surface prior to growth ensures pristine surface conditions that are consistent for all depositions. Analysis of scanning tunneling microscopy (STM) images confirms the relation of RHEED oscillations to ideal layer-by-layer growth, but points to an important refinement: a simple step-density model, taking into account only the steps enclosing the islands, is not sufficient to explain the damping of the RHEED specular spot intensity. The results reveal that the 1D interfaces between two inherently different reconstructions coexisting on the island surfaces need to be included for a quantitative agreement between RHEED and STM. Finally it is shown how the island densities, sizes, and shapes can be adjusted by choosing appropriate growth temperatures and pulse rates.

2. Experimental apparatus

Experiments have been performed in a PLD system from Twente Solid State Technology B.V. (see Fig. 1 for a schematic of the system). The system allows for rapid *in-situ* transfer of as-deposited samples from the deposition chamber to a surface analysis system combining STM (SPECS Aarhus 150), X-ray photoelectron spectroscopy (non-monochromatic Mg or Al Kα source, SPECS Phoibos 100), low-energy He^+ ion scattering spectroscopy (SPECS IQE 12/38 ion source), and low-energy electron diffraction (LEED; Omicron). The PLD system consists of an ultra-high vacuum (UHV) chamber for deposition with a base pressure below 4×10^{-10} mbar after bake-out, and an adjacent transfer chamber with a base pressure below 1×10^{-10} mbar. It should be mentioned that the base pressure of the deposition chamber after repeated growth in up to 1 mbar background pressure rises to about 1×10^{-9} mbar with H_2, H_2O, O_2, and CO_2 being the main components of the residual gas. Moving the as-deposited substrates from the PLD chamber *via* the transfer chamber to the analysis chamber takes about 30 s. The transfer chamber also hosts a sample storage system. For ablation, a pulsed UV laser (Coherent COMPexPro 205F) with a wavelength of 248 nm, a typical pulse duration of 20–50 ns, and a pulse-to-pulse standard deviation of the beam energy better than 0.6% is used. A top-hat beam profile is created by placing a mask in the central part of the beam [24]. The distance of the mask to the focusing lens determines the demagnification, and the lens position is used to precisely adjust the focusing and the resulting spot size on the target. For a clean, UHV compatible way of determining the size and shape of the laser spot, the laser is directed onto a polycrystalline, polished Cu target inside vacuum. The spot size is measured outside of vacuum *via* an optical microscope; here it was set to $1.05 \times 2.35\ mm^2 = 2.47\ mm^2$.

The laser beam passes through an attenuator module (Coherent MicroLas) that allows adjustment of the UV pulse energy. This enables operation of the UV laser with a fixed discharge voltage and therefore a constant beam divergence and pulse duration. The energy density on the target is set by measuring the energy of the UV beam in front of the focusing lens (outside of vacuum with a Coherent EnergyMax USB meter) taking into account an attenuation of the UV light by the lens and the entrance window of 8% each. Up to five targets can be mounted on the detachable target carousel, which can be inserted into the UHV chamber without breaking the vacuum. Here, single-crystalline Nb-doped (0.5 wt.%) $SrTiO_3$ (CrysTec Gmbh) was used as a target. For each deposition, a fresh spot on the target surface is used. To decrease formation of pits during ablation, the target is scanned (~0.4 mm/s)

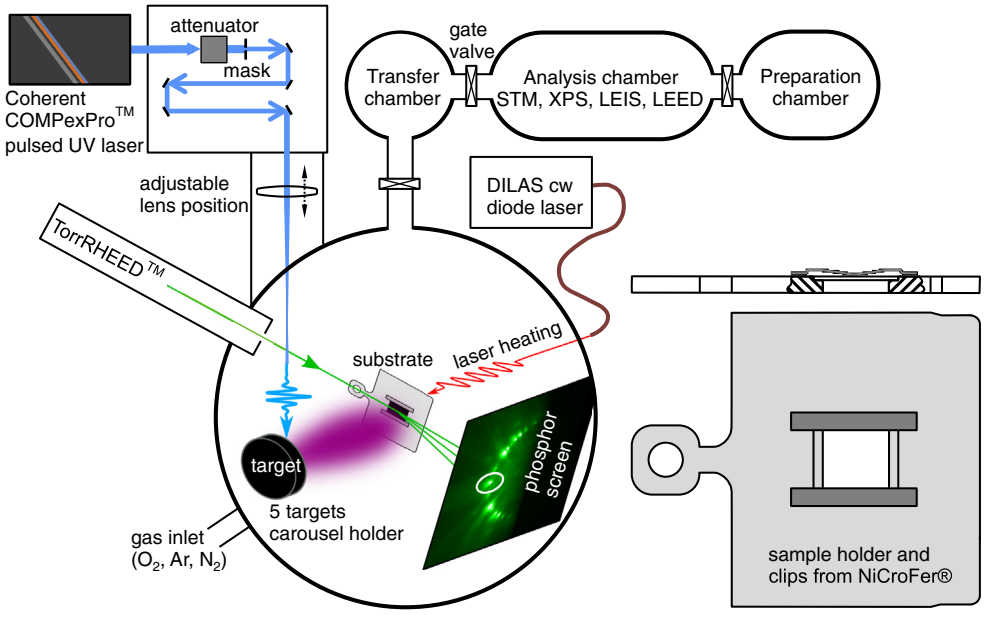

Fig. 1. Schematic illustration of the experimental setup combining PLD growth and surface analysis in connected UHV chambers. Shown in the lower right is the sample holder and sample mounting by spot-welded clips.

along a line resulting in typical ablation areas of around 4.00 mm × 2.35 mm (spot height). The target was grinded and polished regularly to exhibit a pristine surface. The PLD chamber is equipped with a doubly differentially pumped TorrRHEED gun from STAIB Instruments GmbH (beam energy up to 35 keV), which allows monitoring RHEED oscillations in up to 1 mbar oxygen pressure. RHEED oscillations are measured by monitoring the intensity of the specular RHEED spot with a kSA400 acquisition system (camera integration time 16 ms). Prior to each deposition the intensity of the specular spot is maximized by adjusting the tilt of the substrate with respect to the incident RHEED beam. This procedure results in the in-phase condition of diffraction, where beams from neighboring terraces constructively interfere, and the modulation of the specular RHEED spot is dominated by the scattering of electrons by surface steps, *i.e.*, its intensity relates to the step density within the coherence length of the electron beam [25]. The resulting RHEED geometry is in the order of 0.6° grazing incidence of the electron beam parallel to the [1$\bar{1}$0] direction of the substrate surface.

The single-crystalline substrates [5 × 5 × 0.5 mm^3 Nb-doped (0.5 wt.%) $SrTiO_3$(110)] are heated by a collimated continuous-wave infrared (IR) laser (DILAS Compact Evolution; wavelength 980 nm, max. output power 150 W) directed onto the back of the substrate through a hole in the sample plate. The substrates are mounted on Nicrofer® sample plates (Omicron-style design) by spot-welding Nicrofer clips (~0.2 mm thick, ~0.7 mm wide). Nicrofer provides good thermal stability in high oxygen pressure — the sample holders were successfully tested by heating at 1000 °C in up to 50 mbar O_2 pressure. The sample plates were machined with spark-erosion to obtain a pocket — holding the substrate — and a through-hole (see Fig. 1) for laser heating (T = 1000 °C with ~50 W laser output power) in the PLD chamber and electron-beam heating (900 V, 15 mA, T = 1000 °C) in the preparation chamber, respectively. Taking into account the refractive index ($n_{STO}^{980\ nm} \approx 2.32$) [26] and optical conductance ($\sigma_c \approx 150$ S/m) [27] it is estimated that the intensity of the infrared laser light drops to $1/e$ after penetrating ~80 μm into 0.5 wt.% Nb-doped STO. Thus, the IR beam is absorbed at the backside only and does not penetrate through the crystal, avoiding any risk of damaging the UHV chamber. [Transmission of IR light would be a problem when working with undoped insulating substrates.] It should be mentioned that direct heating of the substrate is essential for obtaining a uniform temperature profile, with temperature differences over the whole sample of less than 5 °C. Heating sample plates with no hole — instead of directly heating the sample — resulted in differences of the sample temperature as high as 70 °C as a result of non-uniform thermal contact with the sample plate. At sample temperatures of up to 1000 °C, Ag paint to attach the sample onto the holder has to be avoided due to the high vapor pressure of Ag and risk of contamination by other components of the adhesive. Additionally, direct substrate heating is of advantage to preserve clean conditions in the PLD system as it avoids unnecessary heating of other parts. All temperatures mentioned in the present work were measured with an optical pyrometer (LumaSense Technologies; emissivity 80%) aimed at the substrate surface.

Gases are introduced into the PLD chamber by mass flow controllers (Brooks Instruments) and the accessible and regulated pressure range extends from low 10^{-6} mbar up to 5 mbar. The pressure regulation is implemented either by setting the mass flow controllers (upstream control, at p < 0.1 mbar), or by controlling the pumping conductance by adjusting the position of a butterfly valve (VAT), which bypasses the closed gate valve to the turbo pump (downstream control).

Pressures of up to 5 × 10^{-4} mbar are measured with a Bayard-Alpert ion gauge (VG Scienta) while higher pressures are monitored simultaneously by a Pirani (Pfeiffer) and a capacitive (MKS Baratron) gauge.

The modularly constructed system is mainly controlled by a software from TSST B.V. on a PC, combining all input and output signals, and operational features such as growth recipes and signal logging.

In this work a typical deposition was performed as follows:

- First, the target and the substrate were centered within the red pilot laser of the heating laser, and the UV laser was focused onto the center of the alignment target.
- The pulse energy of the UV laser was adjusted to obtain the required fluence; the deposition pressure was set in the chamber.
- With the shutter in front of the substrate (closed), the target surface was pre-ablated (~150 laser shots) in order to remove all unwanted adsorbates and residues from grinding.
- After the substrate was heated to the deposition temperature (ramp rate 1 K/s), the RHEED beam was aligned with the substrate.
- After this, the deposition took place while the variation of the RHEED intensity was recorded.
- The substrate was then post-annealed at the deposition temperature for 10 min before the temperature was ramped down (1 K/s) and the chamber was pumped to UHV conditions.

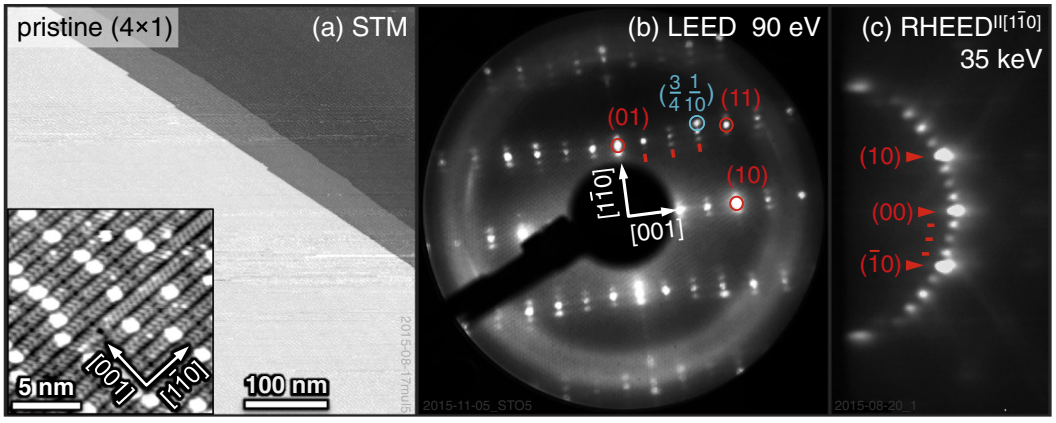

Fig. 2. Characterization of the pristine $SrTiO_3$(110)-(4 × 1) surface. (a) Large-area STM image with a zoom-in view in the inset. Steps are one-unit-cell high. (b) LEED pattern (E = 90 eV) of the pristine surface. Bulk-derived diffraction spots and one spot originating from the surface reconstruction are highlighted with red circles and a small blue circle, respectively. (c) RHEED pattern of the pristine surface (E = 35 keV) with the beam parallel to the surface [1$\bar{1}$0] direction. Integer diffraction spots and those derived from the (4 × 1) reconstruction are highlighted by red arrows and red dashes, respectively. (For interpretation of the references to color in this figure legend, the reader is referred to the web version of this article.)

If not stated otherwise, all depositions were carried out in a background pressure of 3×10^{-2} mbar oxygen, with a UV laser fluence of 2 J/cm^2, and a target-to-sample distance of around 60 mm.

The STM experiments were performed in the connected UHV system with a SPECS Aarhus STM at room temperature (RT), using electrochemically etched W tips. All STM images were acquired in constant-current mode with approximately +2 V sample bias voltage (empty states) and a tunneling current of around 0.2 nA. LEED (Omicron SpectaLEED) was performed in the same analysis chamber with a base pressure below 6×10^{-11} mbar. A more detailed description of the analysis system is found elsewhere [23].

3. Results and Discussion

The homoepitaxial growth on the $SrTiO_3$(110)-(4 × 1) reconstructed surface was followed. The (4 × 1) reconstruction is formed to compensate for the polar instability that arises by the alternate stacking of $(O_2)^{4-}$ and $(SrTiO)^{4+}$ planes, which build up $SrTiO_3$ along the (110) direction [18]. The structure consists of corner-sharing TiO_4 tetrahedra that form a network of six- and ten-membered rings residing on a bulk truncated $(SrTiO)^{4+}$ plane [28,29]. A typical STM image of this surface is shown in the inset of Fig. 2(a). The main panel of Fig. 2(a) shows a large-area STM image of the pristine surface. Atomically-flat terraces of several hundred nanometers width and monolayer step heights (275 pm) can be produced by repeated sputtering (1 keV, 3×10^{-6} mbar Ar^+, 3 μA, 10 min) and annealing (1000 °C, 3×10^{-6} mbar O_2, 1 h) cycles. The surface stoichiometry can be tuned by evaporation of either Sr or Ti metal followed by annealing in oxygen and determines the surface superstructure [30,31]. Prior to all depositions by PLD, the substrate surface was prepared to exhibit predominantly the (4 × 1) reconstruction. Fig. 2(b) and (c) shows typical diffraction patterns of this structure observed by LEED and RHEED, respectively. In LEED, sharp spots indicate a four-times periodicity along the [001] direction and a unit-cell periodicity along [1$\bar{1}$0] (integer order spots highlighted by red circles). The spot highlighted by the blue circle in Fig. 2(b) is at a distance of 11/10 of the reciprocal [1$\bar{1}$0] vector indicating a 10-times periodicity on the surface. It was shown previously that elastic interactions between anti-phase domain boundaries on this surface lead to the stabilization of a regular (4 × 10) superstructure, and that the bright spots [Fig. 2(a) inset] are single Sr adatoms that are inherent to this structure and provide charge compensation for the missing units at domain boundaries [18]. RHEED, acquired with the electron beam incident along the [1$\bar{1}$0] direction, also reveals the four-fold periodicity of the surface structure, see Fig. 2(c). It should be mentioned that for some depositions, the surface prior to growth exhibited a mix of (4 × 1) and (5 × 1) reconstructions. Both, the (4 × 1) and the (5 × 1) reconstruction are part of the homologous series of (n × 1) reconstructions and the two structures appear homogeneously mixed on the surface; there is only a tiny difference in surface composition between these structures [the stoichiometry per surface unit cell for the ideal (n × 1) structures without domain boundaries is $Ti_{(n+2)/n}O_{(3n+4)/n}$] [28]. We therefore expect the effects of the mix of these reconstructions on the diffusion and island nucleation to be negligible.

Fig. 3 shows STM images and corresponding RHEED intensity variations during the growth of the first monolayer (ML). Fig. 3(a) shows the pristine surface in STM. The inset of Fig. 3(a) shows a line profile across the step indicating a single-layer step height. Fig. 3(c)–(h) shows the surface in STM after deposition of submonolayer amounts of STO at 650 °C substrate temperature with 1 Hz pulse repetition rate. RHEED oscillations were recorded during deposition [shown as insets in Fig. 3(c)–(h)]. The number of pulses stated in the insets is applied consecutively, and the substrate was kept at the deposition temperature for an additional 10 min before cool-down and transfer to the surface analysis chamber and STM measurements. For each deposition shown the substrate was freshly re-prepared.

After deposition of one pulse, single-layer-high islands appear on the surface. The considerable drop in the RHEED intensity is consistent with an increased step density on the surface. The islands tend to grow elongated in [1$\bar{1}$0] direction indicating either anisotropic sticking to islands or anisotropic diffusion, with the fast diffusion

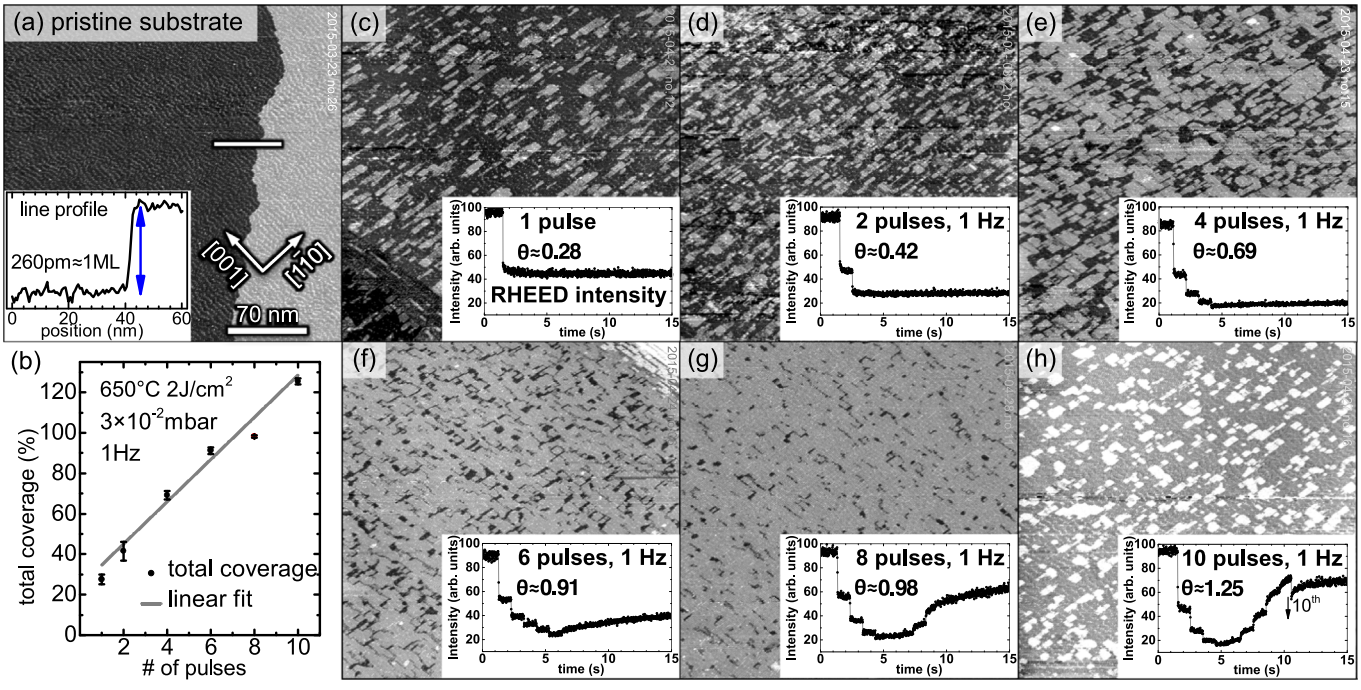

Fig. 3. (a) Large-area STM image of the surface prior to deposition. The inset shows the profile along the white line in (a). (c)–(h) Series of STM images and corresponding RHEED intensity variations during the homoepitaxial growth of one monolayer (ML) on the $SrTiO_3$(110)-(4 × 1) surface. A freshly-prepared substrate was used each time. (b) Area coverage derived from an analysis of STM images and a linear fit to the data.

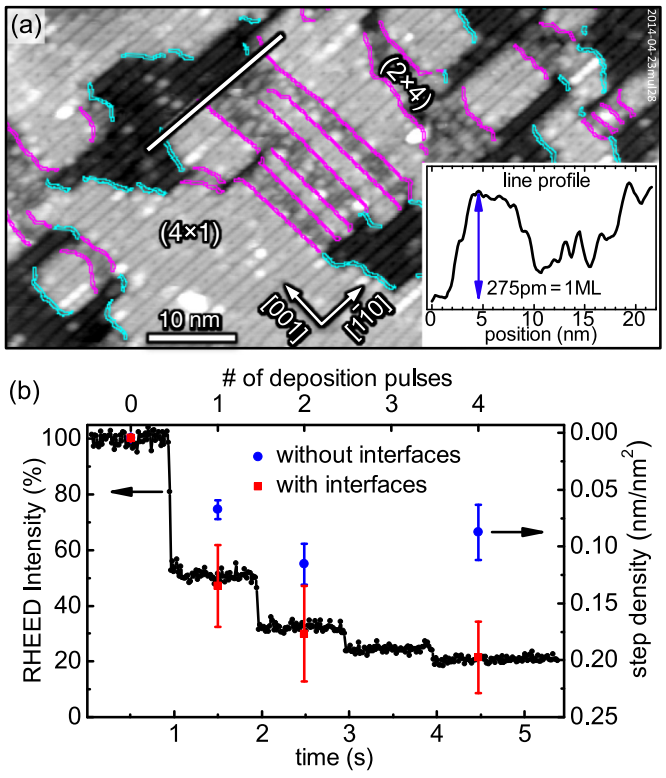

Fig. 4. (a) STM image showing islands after growth of 4 pulses at 650 °C substrate temperature in 3×10^{-2} mbar oxygen. The border of the island and the interfaces between $(n \times 1)$ and (2×4), all parallel to the [001] direction, are highlighted in cyan and magenta, respectively. The inset shows a profile along the line in (a). (b) RHEED intensity overlaid with step density (analyzed from STM images) with (red squares) and without (blue circles) considering the interfaces between the different reconstructions, respectively. Note that the step density axis is inverted.

direction along [1$\bar{1}$0], *i.e.*, parallel to the bright (4×1) rows [*cf.* inset of Fig. 1(a)] [32]. As the number of laser pulses increases, the number and size of islands on the surface increase and the RHEED intensity decreases accordingly. STM images indicate that the coalescence of the islands starts between the 2nd and 4th pulse, where the RHEED intensity reaches its minimum. However, STM analysis of the step density introduced by the circumference of the islands reveals a lower step density after the 4th pulse compared to the 2nd pulse [compare blue circles in Fig. 4(b); note that the scale of the step density is inverted]. According to the step density model [33], this would cause an increased RHEED specular spot intensity at the 4th pulse, compared to the 2nd pulse, but in fact the RHEED specular spot intensity decreases at the 4th pulse. This comparison shows that the steps introduced by the border of the islands alone do not represent a reliable measure of the step density on the surface. High-resolution STM images of the islands nucleated on the surface show that the islands often consist of two inherently different reconstructions. While the larger portion of the island surfaces exhibits the same reconstruction as the underlying substrate layer, *i.e.*, a mix of (4×1) and (5×1) reconstructions, parts of the islands exhibit the (2×4) reconstruction [30], see Fig. 4(a). As can be seen in the line profile in the inset of Fig. 4(a), the (2×4) reconstruction shows an apparent height of around half a monolayer. Since (2×4) regions appear as depressions with respect to the $(n \times 1)$ areas at all tunneling conditions, one can assume that the depressed appearance originates from a topographic height difference, rather than from purely electronic effects. Therefore the linear boundaries between the $(n \times 1)$ and the (2×4) domains [highlighted by magenta lines in Fig. 4(a)] have to be counted as steps when analyzing the step density from STM images for the calculation of the RHEED intensity. Indeed the step density and the RHEED intensity fit very well after considering also the step density introduced by these interfaces [see Fig. 4(b), red squares]. We note that the axis of the step density in Fig. 4(b) has been adjusted to overlay the minimum (0.0046 ± 0.009 nm/nm^2) and the maximum (0.1977 ± 0.0314 nm/nm^2) step densities (with interfaces considered) with the maximum and the minimum RHEED intensities, respectively. This is a reasonable representation because the maximum RHEED intensity should correspond to the minimum step density, and *vice versa*. With this overlay, the scaling of the normalized RHEED intensity, $I(t)$, follows quantitatively the well-known relation to step density as $I(t) = 1\text{-}S(t)/S_{max}$, where $S(t)$ is the step density at a given time (or laser pulse) and S_{max} is the maximum step density achieved when the RHEED intensity is minimum [33]. Lastly, we believe that this is still a simplified model, which entirely neglects possible differences in electron reflectivity of the two different reconstructions on the islands. However, given the successful match between the RHEED intensity and the step density including interfaces, we believe that the steps are the dominant factor behind the RHEED oscillations also on this surface with two different reconstructions.

Upon increasing the number of pulses from 4 to 8 (see Fig. 3), the percolation network is progressively filled, leaving only a few open areas on the surface, and the RHEED intensity increases with each pulse. No 2nd layer islands are formed yet, *i.e.*, the growth follows an ideal layer-by-layer mechanism. The RHEED intensity profile in Fig. 3(h) shows that the 10th pulse reduces the RHEED intensity again and the STM reveals nucleation of the 2nd layer. Thus the amount necessary for the growth of one ML under these conditions lies between 8 and 9 pulses, and one oscillation of the RHEED intensity indeed corresponds to the growth of one ML.

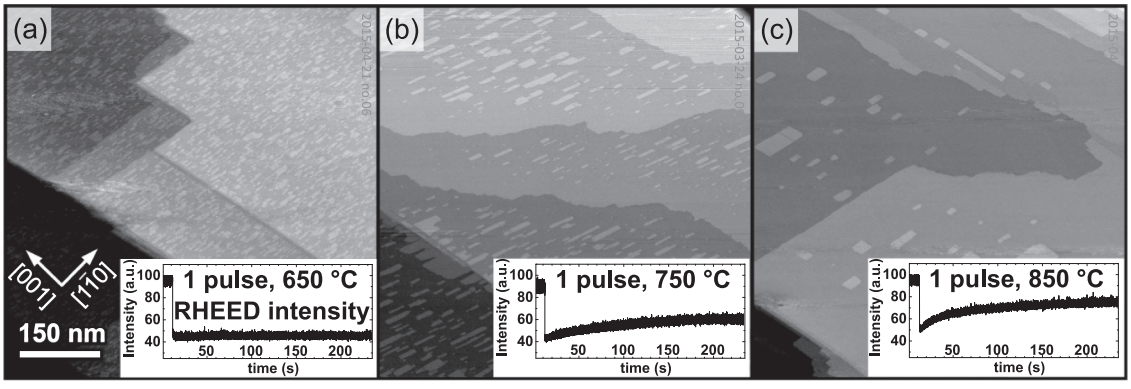

Fig. 5. STM images and corresponding RHEED intensity relaxations of one pulse deposited at substrate temperatures of (a) 650 °C, (b) 750 °C, and (c) 850 °C.

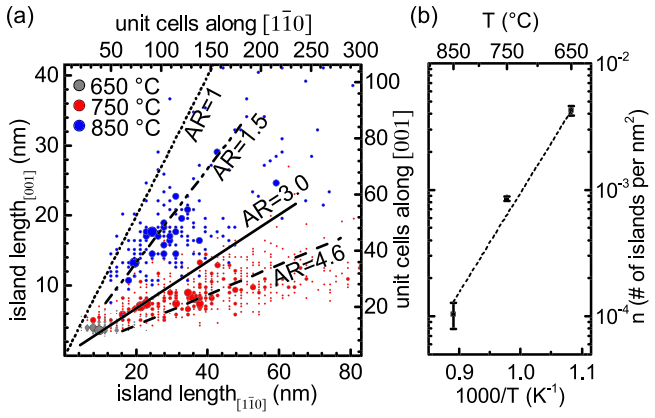

Fig. 6. (a) Distribution of island dimensions after 1 pulse (+ post annealing) at different growth temperatures (Note: only rectangular-shaped islands are counted; coalesced islands with different shapes are neglected). Larger circles indicate higher number of counts. The lines indicate different aspect ratios (AR). (b) Island density derived from analysis of STM images in an Arrhenius plot.

Analysis of the STM images shows that the total deposited amount linearly increases with the number of UV laser pulses [see Fig. 3(b)]. However, it should be mentioned that the linear fit in Fig. 3(b) does not intercept the vertical-axis at zero, indicating an apparent initial coverage of around 25% prior to deposition. This issue is related to the shutter of the PLD system not entirely shadowing the particle flux created during pre-ablation. Indeed, analysis of STM images (not shown) obtained after pre-ablation of the target surface with the shutter in closed position reveal that the terraces are covered by single-layer thick islands, amounting to approximately 0.25 ML. As the relatively large shutter (9×7 cm^2) completely obstructs the sample from the target, particles can bypass it only by scattering multiple times in the background atmosphere. This leads to a Ti enrichment of the impinging flux (lighter plasma constituents scatter more strongly) [13] and the first islands nucleating on the surface will exhibit a slightly different stoichiometry. Indeed, as already mentioned, some of the islands are characterized by a (2×4) structure, surrounded by (4×1)-reconstructed terraces, indicating the incoming flux being partly Ti-rich [30].

Fig. 5 compares the island density after one single pulse at increasing growth temperatures. Prior to each deposition the substrate was again prepared to show a (4×1) reconstructed surface. The insets show the RHEED intensity after growth, when the sample was still kept at the deposition temperature (10 min total before cooling and STM). The STM images show a considerable reduction in the island density when the temperature during growth and annealing is increased first from 650 °C to 750 °C and then to 850 °C. This is reflected also by the relaxation of the RHEED intensity, which recovers considerably faster at higher temperatures. After deposition at 650 °C, the RHEED intensity stays almost constant, meaning that island nucleation takes place much faster than the integration time of the camera (16 ms). The magnitude of the initial drop of the RHEED intensity is comparable for all sample temperatures indicating a similar step density right after deposition. The long-term relaxations visible at higher temperatures therefore indicate a coarsening of the islands, which, at 850 °C, predominantly ends with the attachment of these islands into the terrace steps.

Comparing the deposition after one pulse at 650 °C and 850 °C [see Figs. 5(a) and (c)], the size, the amount, and the aspect ratio of the islands have changed considerably. Fig. 6 provides a quantitative evaluation of the island dimensions (wider circles indicate higher counts) and the island densities. Fig. 6(a) shows that at 650 °C growth temperature, islands preferentially grow elongated along the [1$\bar{1}$0] direction with typical dimensions of around 3.5×10 nm^2. At 750 °C two maxima appear in this plot, *i.e.*, part of the island population exhibits the same aspect ratio [7×23 nm^2, AR $\approx$ 3.0, solid line] as islands nucleated at 650 °C, while another part of the population has grown elongated along [1$\bar{1}$0] (7×38 nm^2, AR $\approx$ 4.6, dashed line). This indicates that 750 °C can be considered a critical temperature, at which ripening during the 10 min post-anneal partly leads to the coalescence of the islands. At 850 °C, the aspect ratio of the islands almost approaches unity

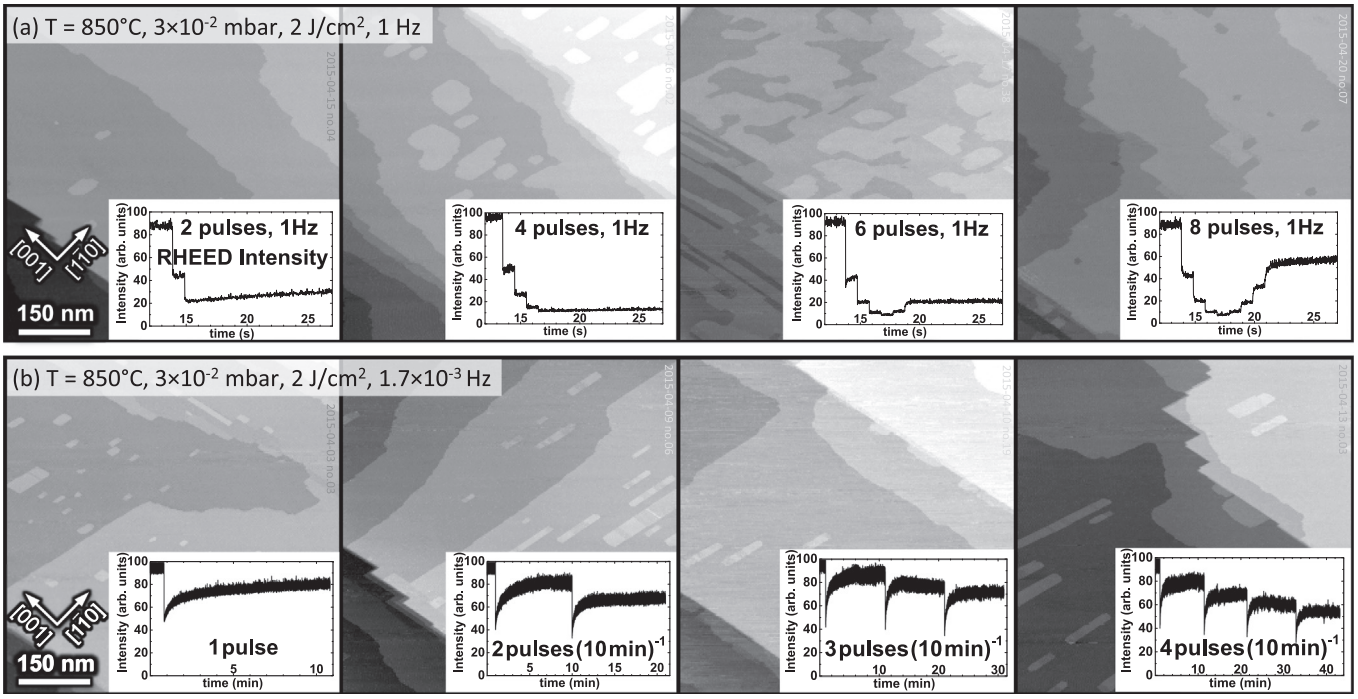

Fig. 7. Comparison of STM images (main panels) and RHEED intensity variations (insets) of sub-monolayer amounts deposited with (a) fast and (b) slow laser repetition rate.

(AR ≈ 1.5, dot-dashed). The AR values of 3.0–4.6 at 650–750 °C indicate preferential diffusion of adspecies along [1$\bar{1}$0], while at 850 °C the diffusion in both directions on the surface is comparable giving rise to AR ≈ 1.5. The number of islands per unit surface area, derived from a quantitative analysis of STM images, shows an exponential increase with the inverse of the growth temperature, as shown in the Arrhenius plot in Fig. 6(b). If the critical nucleus size and the amount of material attached to the steps at higher temperatures were known [34,35], it would be possible to derive diffusion barriers from this plot.

Fig. 7 shows the dependence of the growth mode on the UV laser repetition rate in the homoepitaxial deposition of STO at 850 °C. At 1 Hz repetition rate, layer-by-layer growth is obtained, as can be seen in Fig. 7(a). STM images show a gradual formation of one ML and the corresponding RHEED intensity variation shows nearly one full oscillation after 8 pulses at 1 Hz. A drastic decrease of the growth speed to one pulse every 10 min leads to a predominantly step-flow growth regime [see Fig. 7(b)]. Indeed, RHEED intensity profiles show nearly full relaxation after each laser pulse. STM images reveal an essentially unchanged island density of $(1.3 \pm 0.3) \times 10^{-4}$ islands/nm2 for different numbers of laser pulses.

4. Summary and conclusion

This work exemplifies the possibilities of combining pulsed laser deposition with *in-situ* surface analysis to study as-deposited films. Surface-science measurements impose stringent requirements of chemical purity to all involved processes in sample preparation. The procedures of substrate mounting (spot welding with clips as compared to the use of Ag paint), substrate heating (direct laser heating as compared to passive heating elements), and UV spot size determination (Cu target as compared to thermal paper introduced to UHV) are found as good ways to combine these usually disparate approaches.

It was shown that well-defined $SrTiO_3$(110)-(4 × 1) surfaces can be prepared by pulsed laser deposition. Variations of the RHEED specular spot intensity were related to a quantitative evaluation of the step density on the surface. The quantitative match obtained between the RHEED intensity and step density measured by STM demonstrated that, besides the circumference of the islands, the interfaces between the two different reconstruction phases have to be included in the evaluation of the step density.

Variation of PLD parameters, in particular growth temperature and deposition rate were used to tune the island density and the morphology of the surface while keeping the surface structure on the islands. Maintaining uniform temperature in such an analysis is essential for avoiding the impact of temperature variation on the local island density across the surface. The control of the film structure and morphology should facilitate research on the interaction of chemical species with this surface, and allows studies of the relation of step edges in promoting chemical reactions. The growth mode can be tuned by variation of the temperature, or by large changes of the repetition rate of the UV laser, corresponding to a different time-averaged flux. This dependence can be used when growing materials sensitive to high temperatures or when strong intermixing is expected at elevated temperatures.

Acknowledgments

This work was supported by the Austrian Science Fund FWF (SFB 'Functional Oxide Surfaces and Interfaces FOXSI' Project F 4507-N16 and F 4505-N16) and by the ERC Advanced Grant 'Oxide Surfaces' (Project ERC-2011-ADG_20110209). SG acknowledges partial support by the FWF Doctoral College Solids4Fun, project number W1243.

References

[1] P. Willmott, Deposition of Complex Multielemental Thin Films, Prog. Surf. Sci. 76 (6–8) (2004) 163–217.
[2] G. Koster, Artificially Layered Oxides by Pulsed Laser Deposition, (PhD Thesis) University of Twente, 1999.
[3] M. Schmid, C. Lenauer, A. Buchsbaum, F. Wimmer, G. Rauchbauer, P. Scheiber, G. Betz, P. Varga, High Island Densities in Pulsed Laser Deposition: Causes and Implications, Phys. Rev. Lett. 103 (7) (2009).
[4] A. Atkinson, S. Barnett, R.J. Gorte, J. Irvine, Advanced Anodes for High-Temperature Fuel Cells, Nat. Mater. 3 (1) (2004) 17–27.
[5] E. Dagotto, When Oxides Meet Face to Face, Science 318 (5853) (2007) 1076–1077.
[6] T. Ohsawa, K. Iwaya, R. Shimizu, T. Hashizume, T. Hitosugi, Dependent Local Surface Electronic Structures of Homoepitaxial $SrTiO_3$ Thin Films, J. Appl. Phys. 108 (7) (2010) 073710.
[7] R. Shimizu, K. Iwaya, T. Ohsawa, S. Shiraki, T. Hasegawa, T. Hashizume, T. Hitosugi, Atomic-Scale Visualization of Initial Growth of Homoepitaxial $SrTiO_3$ Thin Film on an Atomically Ordered Substrate, ACS Nano 5 (10) (2011) 7967–7971.
[8] R. Shimizu, T. Ohsawa, K. Iwaya, S. Shiraki, T. Hitosugi, Epitaxial Growth Process of $La_{0.7}Ca_{0.3}MnO_3$ Thin Films on $SrTiO_3$(001): Thickness-Dependent Inhomogeneity Caused by Excess Ti Atoms, Cryst. Growth Des. 14 (4) (2014) 1555–1560.
[9] K. Fuchigami, Z. Gai, T.Z. Ward, L.F. Yin, P.C. Snijders, E.W. Plummer, J. Shen, Tunable Metallicity of the $La_{5/8}Ca_{3/8}MnO_3$(001) Surface by an Oxygen Overlayer, Phys. Rev. Lett. 102 (6) (2009) 066104.
[10] A. Tselev, R.K. Vasudevan, A.G. Gianfrancesco, L. Qiao, P. Ganesh, T.L. Meyer, H.N. Lee, M.D. Biegalski, A.P. Baddorf, S.V. Kalinin, Surface Control of Epitaxial Manganite Films via Oxygen Pressure, ACS Nano 9 (4) (2015) 4316–4327.
[11] T. Ohnishi, M. Lippmaa, T. Yamamoto, S. Meguro, H. Koinuma, Improved Stoichiometry and Misfit Control in Perovskite Thin Film Formation at a Critical Fluence by Pulsed Laser Deposition, Appl. Phys. Lett. 87 (24) (2005) 241919.
[12] D.J. Keeble, S. Wicklein, R. Dittmann, L. Ravelli, R.A. Mackie, W. Egger, Identification of A- and B-Site Cation Vacancy Defects in Perovskite Oxide Thin Films, Phys. Rev. Lett. 105 (22) (2010) 226102.
[13] S. Wicklein, A. Sambri, S. Amoruso, X. Wang, R. Bruzzese, A. Koehl, R. Dittmann, Pulsed Laser Ablation of Complex Oxides: the Role of Congruent Ablation and Preferential Scattering for the Film Stoichiometry, Appl. Phys. Lett. 101 (13) (2012) 131601.
[14] C. Xu, M. Moors, R. Dittmann, Impact of Cation Stoichiometry on the Early Stage of Growth of $SrTiO_3$ Deposited by Pulsed Laser Deposition, Appl. Surf. Sci. 359 (2015) 68–72.
[15] E. Breckenfeld, R. Wilson, J. Karthik, A.R. Damodaran, D.G. Cahill, L.W. Martin, Effect of Growth Induced (Non)Stoichiometry on the Structure, Dielectric Response, and Thermal Conductivity of $SrTiO_3$ Thin Films, Chem. Mater. 24 (2) (2012) 331–337.
[16] D.J. Keeble, S. Wicklein, L. Jin, C.L. Jia, W. Egger, R. Dittmann, Nonstoichiometry Accommodation in $SrTiO_3$ Thin Films Studied by Positron Annihilation and Electron Microscopy, Phys. Rev. B 87 (19) (2013) 195409.
[17] C. Xu, S. Wicklein, A. Sambri, S. Amoruso, M. Moors, R. Dittmann, Impact of the Interplay Between Nonstoichiometry and Kinetic Energy of the Plume Species on the Growth Mode of $SrTiO_3$ Thin Films, J. Phys. D. Appl. Phys. 47 (3, SI) (2013) 034009.
[18] Z. Wang, F. Li, S. Meng, J. Zhang, E.W. Plummer, U. Diebold, J. Guo, Strain-Induced Defect Superstructure on the $SrTiO_3$(110) Surface, Phys. Rev. Lett. 111 (5) (2013) 056101.
[19] Z. Wang, X. Hao, S. Gerhold, Z. Novotný, C. Franchini, E. McDermott, K. Schulte, M. Schmid, U. Diebold, Water Adsorption at the Tetrahedral Titania Surface Layer of $SrTiO_3$(110)-(4 × 1), J. Phys. Chem. C 117 (49) (2013) 26060–26069.
[20] Z. Wang, Z. Zhong, X. Hao, S. Gerhold, B. Stöger, M. Schmid, J. Sanchez-Barriga, A. Varykhalov, C. Franchini, K. Held, et al., Anisotropic Two-Dimensional Electron Gas at $SrTiO_3$(110), Proc. Natl. Acad. Sci. U. S. A. 111 (11) (2014) 3933–3937.
[21] Z. Wang, X. Hao, S. Gerhold, M. Schmid, C. Franchini, U. Diebold, Vacancy Clusters at Domain Boundaries and Band Bending at the $SrTiO_3$(110) Surface, Phys. Rev. B 90 (3) (2014) 035436.
[22] Z. Wang, X. Hao, S. Gerhold, P. Mares, M. Wagner, R. Bliem, K. Schulte, M. Schmid, C. Franchini, U. Diebold, Stabilizing Single Ni Adatoms on a Two-Dimensional Porous Titania Overlayer at the $SrTiO_3$(110) Surface, J. Phys. Chem. C 118 (34) (2014) 19904–19909.
[23] S. Gerhold, M. Riva, Z. Wang, R. Bliem, M. Wagner, J. Osiecki, K. Schulte, M. Schmid, U. Diebold, Nickel-Oxide-Modified $SrTiO_3$(110)-(4 × 1) Surfaces and Their Interaction with Water, J. Phys. Chem. C 119 (35) (2015) 20481–20487.
[24] G. Rijnders, The Initial Growth of Complex Oxides: Study and Manipulation, (PhD Thesis) University of Twente, 2001.
[25] D.H. Blank, G.J. Rijnders, G. Koster, H. Rogalla, *In-Situ* Monitoring by Reflective High Energy Electron Diffraction During Pulsed Laser Deposition, Appl. Surf. Sci. 138–139 (1999) 17–23.
[26] M. Bass, Handbook of Optics vol. II, McGraw-Hill, 1995 33.72 (Table 28).
[27] J.L.M. van Mechelen, D. van der Marel, C. Grimaldi, A.B. Kuzmenko, N.P. Armitage, N. Reyren, H. Hagemann, I.I. Mazin, Electron-Phonon Interaction and Charge Carrier Mass Enhancement in $SrTiO_3$, Phys. Rev. Lett. 100 (22) (2008) 226403.
[28] J.A. Enterkin, A.K. Subramanian, B.C. Russell, M.R. Castell, K.R. Poeppelmeier, L.D. Marks, A Homologous Series of Structures on the Surface of $SrTiO_3$(110), Nat. Mater. 9 (3) (2010) 245–248.
[29] F. Li, Z. Wang, S. Meng, Y. Sun, J. Yang, Q. Guo, J. Guo, Reversible Transition Between Thermodynamically Stable Phases with Low Density of Oxygen Vacancies on the $SrTiO_3$(110) Surface, Phys. Rev. Lett. 107 (3) (2011) 036103.
[30] Z. Wang, F. Yang, Z. Zhang, Y. Tang, J. Feng, K. Wu, Q. Guo, J. Guo, Evolution of the Surface Structures on $SrTiO_3$(110) Tuned by Ti or Sr Concentration, Phys. Rev. B 83 (15) (2011) 155453.

[31] Z. Wang, J. Feng, Y. Yang, Y. Yao, L. Gu, F. Yang, Q. Guo, J. Guo, Cation Stoichiometry Optimization of $SrTiO_3$ (110) Thin Films with Atomic Precision in Homogeneous Molecular Beam Epitaxy, Appl. Phys. Lett. 100 (5) (2012) 051602.
[32] J. Feng, F. Yang, Z. Wang, Y. Yang, L. Gu, J. Zhang, J. Guo, Growth of $SrTiO_3$(110) Film by Oxide Molecular Beam Epitaxy with Feedback Control, AIP Adv. 2 (4) (2012) 041407.
[33] G. Rijnders, D.H. Bland, Growth Kinetics During Pulsed Laser Deposition, in *Pulsed Laser Deposition of Thin Films*, John Wiley & Sons 2007, pp. 177–190 (ch. 8).
[34] T.R. Linderoth, J.J. Mortensen, K.W. Jacobsen, Homoepitaxial Growth of Pt on Pt(100)-Hex: Effects of Strongly Anisotropic Diffusion and Finite Island Sizes, Phys. Rev. Lett. 77 (1) (1996) 87–90.
[35] H. Brune, Microscopic View of Epitaxial Metal Growth: Nucleation and Aggregation, Surf. Sci. Rep. (ISSN: 0167-5729) 31 (4-6) (1998) 125–229.